

Modelling the non-steady peeling of viscoelastic tapes

M. Ceglie,¹ N. Menga,^{1,*} and G. Carbone^{1,2,3}

¹*Department of Mechanics, Mathematics and Management,
Politecnico of Bari, V.le Japigia, 182, 70126, Bari, Italy*

²*Imperial College London, Department of Mechanical Engineering,
Exhibition Road, London SW7 2AZ*

³*CNR - Institute for Photonics and Nanotechnologies U.O.S. Bari,
Physics Department "M. Merlin", via Amendola 173, 70126 Bari, Italy*

Abstract

We present a model to study the non-steady V-shaped peeling of a viscoelastic thin tape adhering to a rigid flat substrate. Geometry evolution and viscoelastic creep in the tape are the main features involved in the process, which allows to derive specific governing equations in the framework of energy balance. Finally, these are numerically integrated following an iterative scheme to calculate the process evolution assuming different controlling conditions (peeling front velocity, peeling force, tape tip velocity). Results show that the peeling behavior is strongly affected by viscoelasticity. Specifically, for a given applied force, the peeling can either be prevented, start and stop after some while, or endlessly propagate, depending on the original undeformed tape geometry. Viscoelasticity also entails that the interface toughness strongly increases when the tape tip is fast pulled, which agrees to recent experimental observations on tougher adhesion of natural systems under impact loads, such as see waves and wind gusts.

Keywords: viscoelasticity, adhesion, peeling, bioinspired, detachment

* Corresponding author: nicola.menga@poliba.it

Nomenclature

$A_t = wd$	Tape cross section
d	Tape thickness
E_0, E_∞	Low and high frequency viscoelastic moduli
\mathcal{J}	Viscoelastic creep function
L_i	initial undeformed length of the non-adhering tape
N	Number of detached elements
P	Peeling force
\mathcal{R}	Viscoelastic relaxation function
s_d	Undeformed peeled tape length
v_c	Peeling front velocity
v_P	Tape tip pulling velocity
v_γ	Reference peeling velocity for adhesion
w	Tape width
W_{in}, W_P, W_{ad}	Power of the internal stress, the peeling force, and the adhesive bonds
γ	Adhesion energy
γ_0	Nominal adhesion energy for $v_c \ll v_\gamma$
ΔL	Total detached tape elongation
Δt	Time step
ε	Tape deformation
θ	Peeling angle
ϕ	Peeling angle at rest
$\kappa = E_\infty/E_0$	Viscoelastic parameter
λ, λ_c	Tape joint coordinate and peeling front location
σ	Tape stress
σ_{cr}	Critical stress value to trigger peeling propagation
τ	Creep time
τ_r	Relaxation time
P_0, θ_0	Critical force and angle for peeling initiation
P_S, θ_S	Long-term steady-state peeling force and angle

1. INTRODUCTION

In modern science, the study of attachment and detachment mechanisms is of practical importance for several applications, such as climbing ability in soft-robotics [1, 2], deposition and removal of coating for specialized interfaces [3], pick-and-place processes in manufacturing [4], self-healing heterogeneous materials for construction [5] and wound dressing for medical industries [6]. Among the others, when dealing with tapes and membranes, as well as fibrils and thin bristles, detachment through mechanical peeling has recently seen a growing interest, quickly becoming the main mechanism for systems such as electro-adhesive [7] and shear-activated nano-structured [8] grippers for objects manipulation made of compliant membranes, band-aids [9] and tunable skin patch [10] to minimize the removal damage of biological tissues [11, 12], spray coatings [13] and transfer printing [14, 15] for flexible cir-

cuits fabrication (also adopting micro-fibrils adhesives[16]), and highly-stretchable structural adhesive tapes [17].

Since the first experimental study by Rivlin dealing with (almost) rigid tapes [18], a dramatic effort has been made to include the effect of tape deformability, with a specific focus on finite strain [19, 20], prestrain [21–23], bending stiffness [24, 25], tape plasticity [26], peel rate dependent adhesion [27–29], and film-substrate interface conditions (e.g., frictional sliding and stick-slip) [30–33]. It is the case, for instance, of energy-based Kendall’s model [34] for elastic tapes peeling, which still represents the benchmark for a broad class of real systems, also including ISO standards for adhesive interfaces [35, 36].

Although peeling itself is a local phenomenon involving a crack propagation at the interface between a layer and a substrate, the macroscopic detachment response is also affected by the global system properties. Those of main interest for similar tribological problems usually are the system geometry [37–39] and the materials rheology [40, 41]. Indeed, studying peeling geometries other than single peeling (in which case the peeling angle equals the force angle) has been recently urged by biomimetics in the attempt, for instance, to mimic [42] the superior locomotion performance of spiders, insects, and reptiles. This depends on the ability to quickly detach their hierarchical-structured toes by exploiting simultaneous peeling fronts propagation, ranging from the macro-scale (e.g., the leg) to the nano-scale (e.g., the toe spatula) [43]. Pugno and coworkers [44, 45] suggested that both the hierarchy and V-shape of the peeling geometry of such systems may play a key role in the overall toughness as multiple peeling fronts coexist, and the peeling angle varies during the detachment process. Later, Lepore et Al. [46] showed that the angles assumed by Tokay geckos at the two characteristic sizes of feet and toes are in excellent agreement with Pugno’s multiple peeling theory predictions. Similarly, V-peeling geometry has been observed in spiders’ webs anchors [47, 48] and byssus threads networks of mussels [49, 50], both showing superior adhesive performance and the ability to withstand heavy winds and waves. Moreover, since peeling has also been successfully employed in characterizing the adhesive properties of materials and adhesives [51], as well as to assess the toughness of interfaces, specific tests (e.g., ASTM Loop Tack test) have been defined relying on the V-peeling geometry to reduce the possible effect of tape bending [52], compared to standard 90° - 180° peel tests.

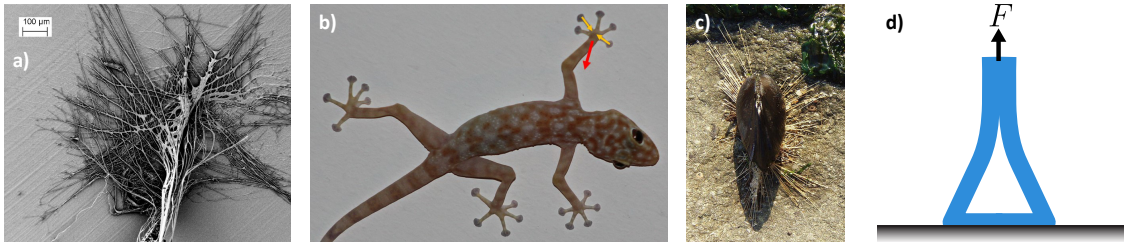


FIG. 1: Examples of V-peeling configurations in natural systems and practical applications: (a) spider web anchors (from Ref. [66]); (b) gecko upside down climbing (adapted from Wikipedia); (c) mussel byssus threads (from Wikipedia); (d) loop tack test schematic (from Ref. [51]).

Nonetheless, existing models for V-peeling geometry only focus on elastic tapes [53], whereas biological systems and commercial tapes usually exhibit a certain degree of viscoelasticity. Indeed, the effect of the materials viscoelasticity and, in turn, of energy dissipation during creep deformation, has been mostly addressed with reference to the single

peeling configuration. Both physical [54–56] and phenomenological [28, 29, 57–59] models have been developed, showing that tape viscoelasticity makes the peeling toughness increase with peel rate. More in detail, Ceglie et Al. [54] have shown that viscoelasticity and local frictional sliding close to the peeling front may lead to unbounded peeling toughness at very low peeling angles, in agreement with existing experimental results [60]. Zhu et Al. [61] focused on the tape visco-hyperelasticity effect on specific zero-degree peeling configuration, showing that for relatively thick tapes the peeling expected peeling force is less sensitive to bulk properties and interfacial adhesion (i.e., surface defects) compared to the case of linear rheology materials.

Viscoelasticity can also be localized in the substrate [62] leading to an "ultra-tough" behavior achievable at specific peel rates. Similar results were also confirmed by Pierro et Al. [63] for a real viscoelastic material with a broader relaxation spectrum and by Zhu et Al. [64] also assuming rate dependent interface adhesion. The substrate rheology is crucial, for instance, when adhesive tapes are removed from human skin, in which case Renvoise et Al. [65] showed that at relatively large peeling velocity the multi-layer nature of human skin can also matter. Surprisingly, less has been done combining rheology effects and V-peeling geometry, although Menga et Al. [66, 67] have shown that, for purely elastic conditions, highly compliant substrates can drastically alter the peeling toughness in V-shaped systems due to the elastic interaction between adjacent peeling fronts.

In this study, we present a model for the V-peeling process of viscoelastic tapes backed onto rigid substrates, aiming at fostering the understanding of the mechanisms underlying the superior performance shown by insect toes, mussels attachment structures, and other biological systems relying on V-shaped peeling geometry in the presence of viscoelasticity, as well as to enhance the accuracy of loop tack test analysis to predict the adhesive performance of real interfaces. Since the process under investigation is non-steady, in Section 2 we set the appropriate theoretical energy-based framework and derive the governing equations for the peeling load, angle and front velocity, while the numerical procedure to integrate such equations and predict the process evolution over time is given in Appendix A and B. Results are presented in Section 3, focusing on three possible peeling procedures (constant peeling front velocity, constant peeling load, and constant velocity of the tape tip), each of which leads to qualitatively different results highlighting the interplay between V-shaped geometry and tape viscoelasticity.

2. FORMULATION

We consider the peeling configuration shown in Fig. 2(a) Double V-shaped peeling scheme of a viscoelastic tape adhering to a rigid substrate. v_c is the peeling front propagation velocity, and v_P is the pulling velocity (i.e., the velocity of the tape tip). (b) By exploiting the system symmetry, the study only focuses on half of the tape. We show three different configurations: the undeformed tape, the tape at peeling propagation start (subscript $_0$), and a generic time instant with peeling force $P(t)$ and angle $\theta(t)$. In the bottom part, we also show qualitative diagrams of the stress σ (blue) and deformation ε (orange) along the tape coordinate λ . figure.caption.6a, where a thin viscoelastic tape of thickness d and width w adhering to a rigid substrate is pulled away by a normal force $2P$. Since two peeling fronts propagate in opposite directions (V-shaped double peeling), the whole process is symmetric with respect to the force direction and the study can be limited to half of the system, as shown in Fig. 2(a) Double V-shaped peeling scheme of a viscoelastic tape adhering to a

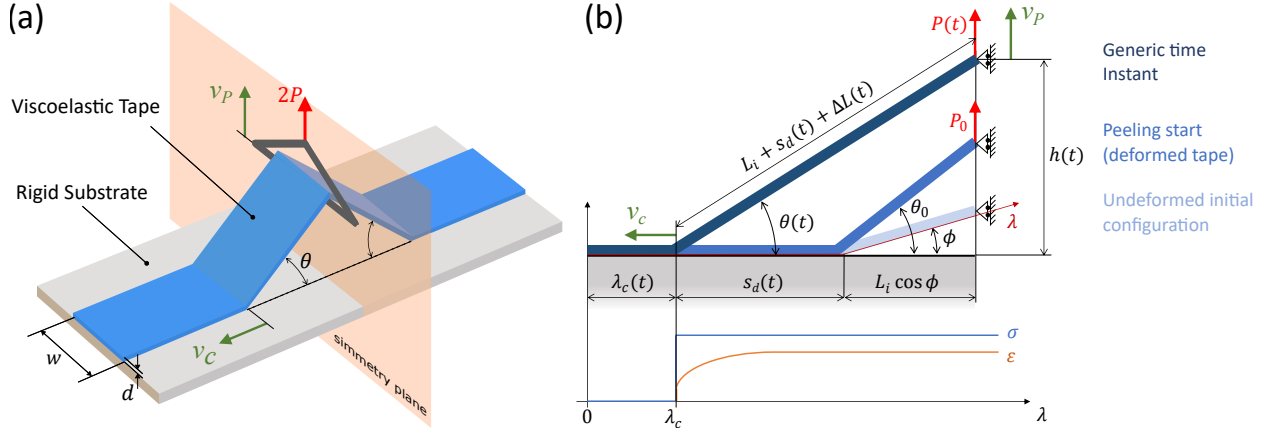


FIG. 2: (a) Double V-shaped peeling scheme of a viscoelastic tape adhering to a rigid substrate. v_c is the peeling front propagation velocity, and v_P is the pulling velocity (i.e., the velocity of the tape tip). (b) By exploiting the system symmetry, the study only focuses on half of the tape. We show three different configurations: the undeformed tape, the tape at peeling propagation start (subscript $_0$), and a generic time instant with peeling force $P(t)$ and angle $\theta(t)$. In the bottom part, we also show qualitative diagrams of the stress σ (blue) and deformation ε (orange) along the tape coordinate λ .

rigid substrate. v_c is the peeling front propagation velocity, and v_P is the pulling velocity (i.e., the velocity of the tape tip). (b) By exploiting the system symmetry, the study only focuses on half of the tape. We show three different configurations: the undeformed tape, the tape at peeling propagation start (subscript $_0$), and a generic time instant with peeling force $P(t)$ and angle $\theta(t)$. In the bottom part, we also show qualitative diagrams of the stress σ (blue) and deformation ε (orange) along the tape coordinate λ .

Before the peeling force P being applied, the (undeformed) non-adhering tape length and angle are L_i and ϕ , respectively. Once the force is applied, at the time instant when the peeling starts to propagate, the tape angle is θ_0 and the peeling force is P_0 . According to Fig. 2(a) Double V-shaped peeling scheme of a viscoelastic tape adhering to a rigid substrate. v_c is the peeling front propagation velocity, and v_P is the pulling velocity (i.e., the velocity of the tape tip). (b) By exploiting the system symmetry, the study only focuses on half of the tape. We show three different configurations: the undeformed tape, the tape at peeling propagation start (subscript $_0$), and a generic time instant with peeling force $P(t)$ and angle $\theta(t)$. In the bottom part, we also show qualitative diagrams of the stress σ (blue) and deformation ε (orange) along the tape coordinate λ . At a generic time t , the peeling front coordinate and velocity are $\lambda_c(t)$ and $v_c(t) = -d\lambda_c/dt$, respectively, with λ being the (undeformed) tape-fixed reference frame. Similarly, $s_d(t) = \int_0^t v_c(t)dt$ is the detached tape length, and the peeling angle $\theta(t)$ is given as

$$\cos \theta = \frac{s_d + L_i \cos \phi}{L_i + s_d + \Delta L}, \quad (1)$$

where $\Delta L(t) = \int_{\lambda_c}^{\lambda_c + s_d + L_i} \varepsilon(\lambda, t) d\lambda$ is the elongation of the overall non-adhering tape, with $\varepsilon(\lambda, t)$ being the extensional deformation field in the tape.

The instantaneous energy balance governing the peeling process is

$$W_P + W_{in} + W_{ad} = 0, \quad (2)$$

where $W_P(t)$ is the work per unit time done by the peeling force $P(t)$, $W_{in}(t)$ is the work per unit time done by the internal stress field, and $W_{ad}(t)$ is the rate of the surface adhesion energy. In Eq. (2equation.2.2), minor energy contributions ascribable to acoustic emissions and heat transfer are neglected, as well as dynamic and inertial effects which might lead to stick-slip unstable delamination [68–72]. Moreover, we assume a fully stuck adhesion between the tape and the rigid substrate in the adhering region, thus no friction energy dissipation occurs due to relative sliding, as instead considered in Refs. [33, 54].

The term $W_{in}(t)$ is associated with both the rate of elastic energy stored in the detached tape and the viscoelastic energy loss occurring during the tape relaxation. Large deformations can be reasonably expected for soft polymeric tapes; however, both numerical [20] and experimental [60] studies have clearly shown that real systems exhibiting strains as large as beyond 60% can still be both qualitatively and quantitatively described in linear theory approximation, especially at relatively large peeling angles [73]. Similar results are confirmed for visco-hyperelastic tapes [61], where qualitatively different behaviors are expected only beyond approximately 100% strain value. Moreover, we assume purely extensional stress $\sigma(\lambda, t)$ and deformation $\varepsilon(\lambda, t)$ fields in the tape, as experiments have shown that bending effects vanish for very thin tapes [74] (i.e., the tape bending stiffness depends on d^3). Therefore, we have

$$W_{in} = -A_t \int_{\lambda_c}^{\lambda_c + L_i + s_d} \sigma(\lambda, t) \frac{\partial \varepsilon}{\partial t}(\lambda, t) d\lambda, \quad (3)$$

with $\varepsilon(\lambda, t) = \sigma(\lambda, t) = 0$ for $\lambda < \lambda_c$ (adhering tape) and $\sigma(\lambda, t) = \sigma(t) = P/(A_t \sin \theta)$ for $\lambda > \lambda_c$ (detached tape). In the peeling section (i.e., for $\lambda = \lambda_c$), a step change of the stress occurs [54], so that

$$\sigma(\lambda, t) = \sigma(t) \mathcal{H}[\lambda - \lambda_c(t)], \quad (4)$$

where \mathcal{H} is the Heaviside step function. In the framework of linear viscoelasticity, the deformation field within the tape is given by

$$\varepsilon(\lambda, t) = \int_{-\infty}^t \mathcal{J}(t - t') \frac{\partial \sigma}{\partial t'}(\lambda, t') dt', \quad (5)$$

where \mathcal{J} is the viscoelastic creep function which, for a single characteristic creep time τ , is given by

$$\mathcal{J}(t) = \frac{1}{E_0} - \frac{e^{-t/\tau}}{E_1}, \quad (6)$$

where $E_1^{-1} = E_0^{-1} - E_\infty^{-1}$, with E_0 and E_∞ being the low and high frequency viscoelastic moduli, respectively.

The term $W_P(t)$ in Eq. (2equation.2.2) is given by

$$W_P = P v_P = \sigma A_t v_P \sin \theta, \quad (7)$$

where

$$v_P = \frac{dh}{dt} = v_c \tan \theta + \frac{s_d + L_i \cos \phi}{\cos^2 \theta} \dot{\theta} \quad (8)$$

is the pulling velocity (see Fig. 2(a) Double V-shaped peeling scheme of a viscoelastic tape adhering to a rigid substrate. v_c is the peeling front propagation velocity, and v_P is the pulling velocity (i.e., the velocity of the tape tip). (b) By exploiting the system symmetry, the study only focuses on half of the tape. We show three different configurations: the undeformed tape, the tape at peeling propagation start (subscript $_0$), and a generic time instant with peeling force $P(t)$ and angle $\theta(t)$. In the bottom part, we also show qualitative diagrams of the stress σ (blue) and deformation ε (orange) along the tape coordinate λ .figure.caption.6).

Finally, in Eq. (2equation.2.2), $W_{ad}(t)$ represents the energy per unit time associated with the rupture of interfacial bonds between the tape and the rigid substrate; being γ the energy of adhesion (also called Dupre's energy), we have

$$W_{ad} = -v_c w \gamma. \quad (9)$$

The adhesion energy γ might, in general, depend on the peeling velocity, as reported by several experiments [15, 28, 29, 59]. This is usually ascribed to viscoelastic non-conservative (stiffening) effects in the tape close to the peeling front, as recently predicted in Ref. [54]. Here, we precisely model the tape viscoelastic creep, thus the latter effect is intrinsically accounted for. However, as pointed out by Marin & Derail [75] with *ad hoc* tests on inextensible tapes, velocity-dependent power loss is also localized in the thin adhesive layer between the tape and the substrate, with γ given by the following power-law

$$\gamma = \gamma_0 \left[1 + \left(\frac{v_c}{v_\gamma} \right)^n \right], \quad (10)$$

where γ_0 is the nominal adhesion energy for $v_c \ll v_\gamma$, with v_γ being a reference peeling velocity, and n being a constant which depends on the properties of the adhesive (typically in a range of 0.3 – 0.7) [15, 59, 75].

At any given time t , Eqs. (1equation.2.1, 2equation.2.2) allow to calculate the critical condition for peeling propagation.

To set the range of validity of the present model, we observe that the real deformation process occurring across the peeling front is continuous and cannot be formally represented by a step-change in the stress field. Nonetheless, physical arguments suggest that the length of the region undergoing the stress increase from 0 to σ is of the same order of magnitude as the tape thickness d [62, 67], which results in a local excitation frequency $\omega \approx v_c/d$ and allows to identify three different qualitative behaviors across the peeling section. For $v_c \ll d/\tau$ (i.e., $\omega \ll 1/\tau$), the tape behaves almost elastically, with elastic modulus approaching the low-frequency modulus E_0 . Since no viscoelastic dissipation occurs, this case is clearly out of the scope of this study, and the corresponding peeling behavior follows the elastic predictions given in Refs. [44, 76]. For $v_c \approx d/\tau$ (i.e., $\omega \approx 1/\tau$), the tape response strongly depends on the specific deformation process across the peeling front (small-scale energy dissipation cannot be neglected), and a local *ad hoc* solid mechanics formulation is required to model the peeling. Finally, the third case is the one of interest for the present model, as for $v_c \gg d/\tau$ (i.e., $\omega \gg 1/\tau$) the tape behavior is elastic across the peeling section with high frequency elastic modulus E_∞ , and viscoelastic losses are localized in the non-adhering tape (large-scale). Daily-life adhesive tapes are commonly very thin, with a corresponding threshold velocity usually being in the range of $d/\tau \approx 10 - 100 \mu\text{m/s}$, which makes the third case of most relevant practical interest.

2.1. Steady-state long-term propagation limit

After the initial transient regime, the elastic V-peeling process asymptotically approaches a steady-state regime in the long-term limit [76]. In the viscoelastic case, a similar behavior is expected for $t \gg \tau$ and $s_d \gg L_i$, which corresponds to complete viscoelastic relaxation along the tape. In this case, steady-state conditions occurs with $\theta(t) \approx \theta_S$, $\sigma(\lambda, t) \approx \sigma_S = P_S/(A_t \sin \theta_S)$, and $\varepsilon(\lambda, t) \approx \varepsilon_S = \sigma_S/E_0$, while the energy balance equation recovers the viscoelastic single peeling form [54] as

$$\frac{\sigma_S^2}{2E_\infty} + \sigma_S (1 - \cos \theta_S) - \frac{\gamma}{d} = 0, \quad (11)$$

where $\gamma = \gamma(v_c)$ is given by Eq. (10equation.2.10). Moreover, since $s_d \gg L_i$, Eq. (1equation.2.1) can be rewritten as

$$\frac{1 - \cos \theta_S}{\cos \theta_S} = \frac{\sigma_S}{E_0}. \quad (12)$$

Furthermore, since $\dot{\theta}_S \approx 0$, Eq. (8equation.2.8) gives

$$v_P = v_c \tan \theta_S. \quad (13)$$

Notably, under force-controlled conditions (i.e., given $P = P_S$), Eqs. (11equation.2.11, 12equation.2.12, 10equation.2.10) allow to calculate the peeling front velocity v_c and, through Eq. (13equation.2.13), the pulling velocity v_P . On the contrary, under velocity-controlled conditions (i.e., given v_c or v_P), the value of P_S can be calculated by Eqs. (11equation.2.11, 12equation.2.12, 10equation.2.10).

3. RESULTS AND DISCUSSION

In this section, we discuss the peeling behavior resulting from Eqs. (1equation.2.1, 2equation.2.2), which can be numerically solved by following the procedure outlined in Appendix Asection*.17. To simplify the analysis of the results, we refer to dimensionless quantities, i.e. $\tilde{t} = t/\tau$, $\tilde{\gamma} = \gamma/E_0 d$, $\tilde{v}_c = v_c \tau/d$, $\tilde{v}_P = v_P \tau/d$, $\tilde{P} = P/dwE_0 = \sigma \sin \theta/E_0$. In our calculations, we consider a tape of thickness $d \approx 100 \mu\text{m}$ with initial non-adhering length $L_i = 100d$. The tape material is viscoelastic with low-frequency modulus $E_0 = 10 \text{ MPa}$ and creep time $\tau = 1 \text{ s}$. Marin and Deraill [75] measured the peeling force P as a function of the peeling velocity v_c for real adhesives with inextensible aluminum backing, and Rivlin peeling theory [18] allows to calculate the corresponding effect of v_c on the adhesion energy γ . Since no viscoelastic relaxation occurs, the latter effect is only ascribable to non-conservative phenomena localized in the very proximity of the peeling front. According to their results, we set $v_\gamma \approx 10^{-3} \text{ m/s}$, $\gamma_0 \approx 20 \text{ J/m}^2$, and $n = 0.5$ in Eq. 10equation.2.10, whose corresponding dimensionless quantities are $\tilde{v}_\gamma = v_\gamma \tau/d = 10$ and $\tilde{\gamma}_0 = \gamma_0/E_0 d = 0.02$.

Results are presented considering three different controlling parameters, corresponding to specific physical scenarios: (i) peeling propagation occurring at constant peeling front velocity v_c ; (ii) the case of a constant peeling force P applied at the tape tip; and (iii) the case of the tape tip pulled at constant velocity v_P .

3.1. Constant peeling front velocity

We firstly consider the peeling process occurring at constant peeling front velocity v_c . This case corresponds to time-varying values of both the peeling force P and pulling velocity v_P , thus resulting harder to be straightforwardly associated with common applications. However, since v_c also represents the length of undeformed tape that detaches the substrate per unit time and, once deformed, undergoes viscoelastic relaxation, fundamental insight on the interplay between peeling propagation and tape viscoelasticity.

With reference to Fig. 2(a) Double V-shaped peeling scheme of a viscoelastic tape adhering to a rigid substrate. v_c is the peeling front propagation velocity, and v_P is the pulling velocity (i.e., the velocity of the tape tip). (b) By exploiting the system symmetry, the study only focuses on half of the tape. We show three different configurations: the undeformed tape, the tape at peeling propagation start (subscript $_0$), and a generic time instant with peeling force $P(t)$ and angle $\theta(t)$. In the bottom part, we also show qualitative diagrams of the stress σ (blue) and deformation ε (orange) along the tape coordinate λ . figure.caption.6b, we assume that the peeling front propagation starts with velocity v_c at time $t = 0$ under the action of the critical force P_0 , which is instantaneously applied. At this time, the tape deformation and angle undergo a step-change, varying from $\varepsilon = 0$ and ϕ at time $t \rightarrow 0^-$ to $\varepsilon = \sigma_0/E_\infty$ and θ_0 at time $t \rightarrow 0^+$. As a consequence, no viscoelastic loss occurs in the non-adhering tape at $t = 0$, and the critical values of σ_0 and θ_0 for peeling initiation are given by Kendall's equation [34, 66, 67]

$$\frac{\sigma_0^2}{2E_\infty} + \sigma_0 (1 - \cos \theta_0) - \frac{\gamma}{d} = 0, \quad (14)$$

and, from Eq. (1equation.2.1) with $s_d = 0$

$$\frac{\cos \phi - \cos \theta_0}{\cos \theta_0} = \frac{\sigma_0}{E_\infty}. \quad (15)$$

Finally, the critical force is calculated as $P_0 = A_t \sigma_0 \sin \theta_0$. For $t > 0$, the peeling process evolution follows Eqs. (1equation.2.1, 2equation.2.2) and is calculated by exploiting the numerical procedure outlined in Appendix Asection*.17.

Comparing the critical peeling force P_0 with the long-term limit P_S allows to differentiate from toughening and weakening overall peeling behaviors. This is done in the top row of Fig. 3Top row: the initial \tilde{P}_0 and long-term \tilde{P}_S dimensionless peeling force as functions of the dimensionless adhesion energy $\tilde{\gamma}_0$ (a), the viscoelastic parameter $\kappa = E_\infty/E_0$ (b), and the dimensionless peeling front velocity \tilde{v}_c (c). In figure (c), the rate-dependent dimensionless adhesion energy $\tilde{\gamma}$ is also shown for comparison (dashed line). Notably, $\kappa = 1$ corresponds to elastic tapes. Bottom row: the time-history of the normalized peeling force \tilde{P}/\tilde{P}_S (d) and peeling angle θ (e) for different values of the dimensionless peeling front velocity \tilde{v}_c and initial undeformed configurations. Non-monotonic behavior occurs in the red regions, i.e. for $t \approx \tau$. Transient diagrams \tilde{P} versus θ are shown for different values of \tilde{v}_c and for $\phi = 30^\circ$ (f) and $\phi = 45^\circ$ (g). Blue and red curves represent the starting condition and the steady-state limit, respectively. Black arrows indicate the time evolution of the process.figure.caption.10, where we consider the effect of (a) the dimensionless adhesion energy $\tilde{\gamma}_0$, (b) the viscoelastic parameter $\kappa = E_\infty/E_0$, and (c) the dimensionless peeling front velocity \tilde{v}_c . While in the elastic V-peeling case, the toughest behavior always occurs in

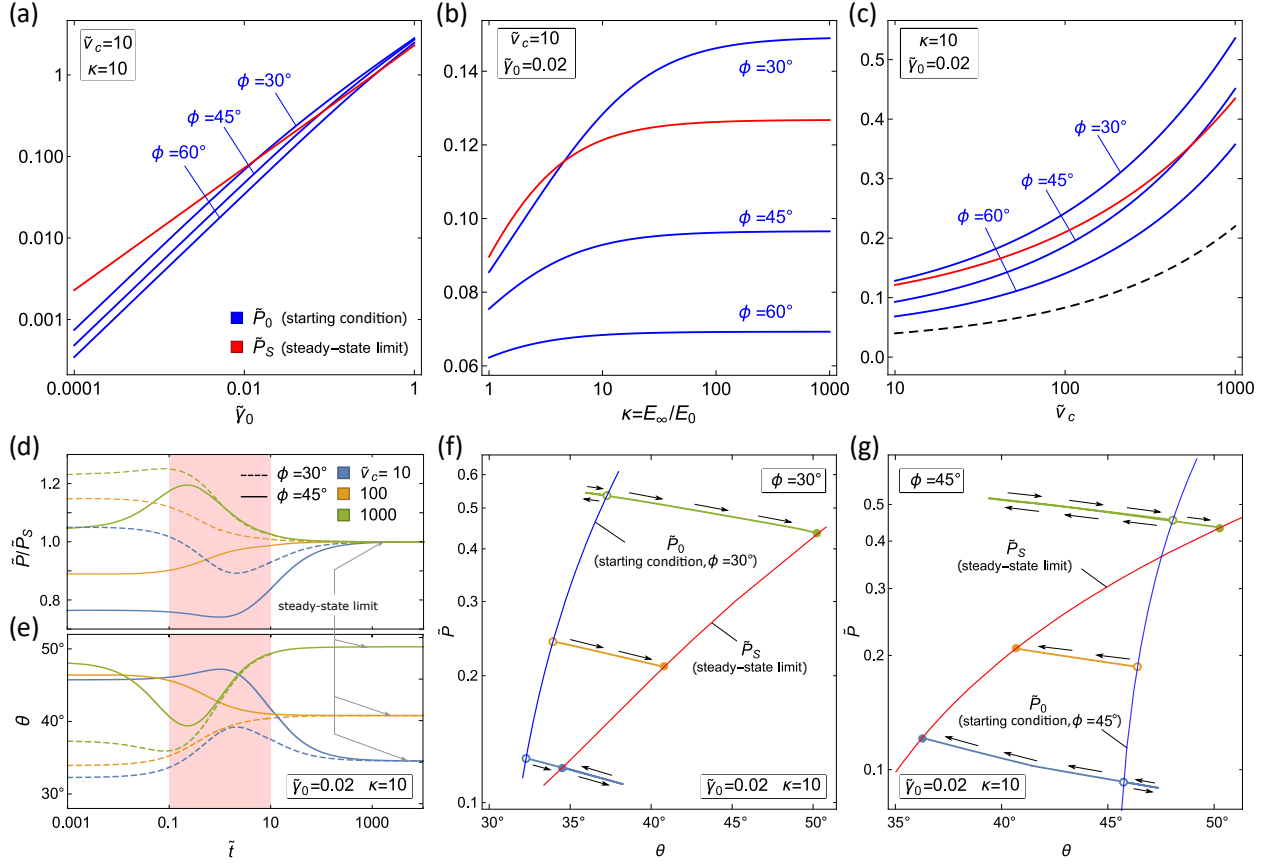


FIG. 3: Top row: the initial \tilde{P}_0 and long-term \tilde{P}_S dimensionless peeling force as functions of the dimensionless adhesion energy $\tilde{\gamma}_0$ (a), the viscoelastic parameter $\kappa = E_\infty/E_0$ (b), and the dimensionless peeling front velocity \tilde{v}_c (c). In figure (c), the rate-dependent dimensionless adhesion energy $\tilde{\gamma}$ is also shown for comparison (dashed line). Notably, $\kappa = 1$ corresponds to elastic tapes. Bottom row: the time-history of the normalized peeling force \tilde{P}/\tilde{P}_S (d) and peeling angle θ (e) for different values of the dimensionless peeling front velocity \tilde{v}_c and initial undeformed configurations. Non-monotonic behavior occurs in the red regions, i.e. for $t \approx \tau$. Transient diagrams \tilde{P} versus θ are shown for different values of \tilde{v}_c and for $\phi = 30^\circ$ (f) and $\phi = 45^\circ$ (g). Blue and red curves represent the starting condition and the steady-state limit, respectively. Black arrows indicate the time evolution of the process.

the steady-state limit, as clearly shown for $\kappa = 1$ in Fig. 3. Top row: the initial \tilde{P}_0 and long-term \tilde{P}_S dimensionless peeling force as functions of the dimensionless adhesion energy $\tilde{\gamma}_0$ (a), the viscoelastic parameter $\kappa = E_\infty/E_0$ (b), and the dimensionless peeling front velocity \tilde{v}_c (c). In figure (c), the rate-dependent dimensionless adhesion energy $\tilde{\gamma}$ is also shown for comparison (dashed line). Notably, $\kappa = 1$ corresponds to elastic tapes. Bottom row: the time-history of the normalized peeling force \tilde{P}/\tilde{P}_S (d) and peeling angle θ (e) for different values of the dimensionless peeling front velocity \tilde{v}_c and initial undeformed configurations. Non-monotonic behavior occurs in the red regions, i.e. for $t \approx \tau$. Transient diagrams \tilde{P} versus θ are shown for different values of \tilde{v}_c and for $\phi = 30^\circ$ (f) and $\phi = 45^\circ$ (g). Blue and red curves represent the starting condition and the steady-state limit, respectively. Black

arrows indicate the time evolution of the process.figure.caption.10b where $P_S > P_0$, the same principle cannot be generalized to the viscoelastic case, where the value of both P_0 and P_S depends on the tape relaxation process and, as a consequence, on the specific combination of the parameters $\tilde{\gamma}_0$, κ , and \tilde{v}_c , as shown in Figs. 3Top row: the initial \tilde{P}_0 and long-term \tilde{P}_S dimensionless peeling force as functions of the dimensionless adhesion energy $\tilde{\gamma}_0$ (a), the viscoelastic parameter $\kappa = E_\infty/E_0$ (b), and the dimensionless peeling front velocity \tilde{v}_c (c). In figure (c), the rate-dependent dimensionless adhesion energy $\tilde{\gamma}$ is also shown for comparison (dashed line). Notably, $\kappa = 1$ corresponds to elastic tapes. Bottom row: the time-history of the normalized peeling force \tilde{P}/\tilde{P}_S (d) and peeling angle θ (e) for different values of the dimensionless peeling front velocity \tilde{v}_c and initial undeformed configurations. Non-monotonic behavior occurs in the red regions, i.e. for $t \approx \tau$. Transient diagrams \tilde{P} versus θ are shown for different values of \tilde{v}_c and for $\phi = 30^\circ$ (f) and $\phi = 45^\circ$ (g). Blue and red curves represent the starting condition and the steady-state limit, respectively. Black arrows indicate the time evolution of the process.figure.caption.10a,b,c. Moreover, according to Eqs. (14equation.3.14-15equation.3.15), the critical starting force P_0 depends on the undeformed tape angle ϕ , specifically leading to tougher peeling initiation with ϕ reducing. In agreement with theoretical [34] and experimental results [77], stiffer tapes entail higher peeling forces, as shown in Fig. 3Top row: the initial \tilde{P}_0 and long-term \tilde{P}_S dimensionless peeling force as functions of the dimensionless adhesion energy $\tilde{\gamma}_0$ (a), the viscoelastic parameter $\kappa = E_\infty/E_0$ (b), and the dimensionless peeling front velocity \tilde{v}_c (c). In figure (c), the rate-dependent dimensionless adhesion energy $\tilde{\gamma}$ is also shown for comparison (dashed line). Notably, $\kappa = 1$ corresponds to elastic tapes. Bottom row: the time-history of the normalized peeling force \tilde{P}/\tilde{P}_S (d) and peeling angle θ (e) for different values of the dimensionless peeling front velocity \tilde{v}_c and initial undeformed configurations. Non-monotonic behavior occurs in the red regions, i.e. for $t \approx \tau$. Transient diagrams \tilde{P} versus θ are shown for different values of \tilde{v}_c and for $\phi = 30^\circ$ (f) and $\phi = 45^\circ$ (g). Blue and red curves represent the starting condition and the steady-state limit, respectively. Black arrows indicate the time evolution of the process.figure.caption.10b; nonetheless, at very large values of κ both P_0 and P_S are almost constant and the Rivlin [18] solution for rigid tapes is asymptotically approached.

The bottom row of Fig. 3Top row: the initial \tilde{P}_0 and long-term \tilde{P}_S dimensionless peeling force as functions of the dimensionless adhesion energy $\tilde{\gamma}_0$ (a), the viscoelastic parameter $\kappa = E_\infty/E_0$ (b), and the dimensionless peeling front velocity \tilde{v}_c (c). In figure (c), the rate-dependent dimensionless adhesion energy $\tilde{\gamma}$ is also shown for comparison (dashed line). Notably, $\kappa = 1$ corresponds to elastic tapes. Bottom row: the time-history of the normalized peeling force \tilde{P}/\tilde{P}_S (d) and peeling angle θ (e) for different values of the dimensionless peeling front velocity \tilde{v}_c and initial undeformed configurations. Non-monotonic behavior occurs in the red regions, i.e. for $t \approx \tau$. Transient diagrams \tilde{P} versus θ are shown for different values of \tilde{v}_c and for $\phi = 30^\circ$ (f) and $\phi = 45^\circ$ (g). Blue and red curves represent the starting condition and the steady-state limit, respectively. Black arrows indicate the time evolution of the process.figure.caption.10 shows the peeling transient evolution from start to steady-state behavior. The most important feature is that V peeling of viscoelastic tapes may present non-monotonic trends of both θ and \tilde{P} , in contrast with results achieved for the elastic case in Refs. [66, 67, 76]. More in detail, focusing on 3Top row: the initial \tilde{P}_0 and long-term \tilde{P}_S dimensionless peeling force as functions of the dimensionless adhesion energy $\tilde{\gamma}_0$ (a), the viscoelastic parameter $\kappa = E_\infty/E_0$ (b), and the dimensionless peeling front velocity \tilde{v}_c (c). In figure (c), the rate-dependent dimensionless adhesion energy $\tilde{\gamma}$ is also shown for comparison (dashed line). Notably, $\kappa = 1$ corresponds to elastic tapes. Bottom row: the

time-history of the normalized peeling force \tilde{P}/\tilde{P}_S (d) and peeling angle θ (e) for different values of the dimensionless peeling front velocity \tilde{v}_c and initial undeformed configurations. Non-monotonic behavior occurs in the red regions, i.e. for $t \approx \tau$. Transient diagrams \tilde{P} versus θ are shown for different values of \tilde{v}_c and for $\phi = 30^\circ$ (f) and $\phi = 45^\circ$ (g). Blue and red curves represent the starting condition and the steady-state limit, respectively. Black arrows indicate the time evolution of the process. figure.caption.10e, given the undeformed tape angle ϕ , the tape angle at peeling start θ_0 increases with \tilde{v}_c , as expected from Eq. (15equation.3.15) and Fig. 3Top row: the initial \tilde{P}_0 and long-term \tilde{P}_S dimensionless peeling force as functions of the dimensionless adhesion energy $\tilde{\gamma}_0$ (a), the viscoelastic parameter $\kappa = E_\infty/E_0$ (b), and the dimensionless peeling front velocity \tilde{v}_c (c). In figure (c), the rate-dependent dimensionless adhesion energy $\tilde{\gamma}$ is also shown for comparison (dashed line). Notably, $\kappa = 1$ corresponds to elastic tapes. Bottom row: the time-history of the normalized peeling force \tilde{P}/\tilde{P}_S (d) and peeling angle θ (e) for different values of the dimensionless peeling front velocity \tilde{v}_c and initial undeformed configurations. Non-monotonic behavior occurs in the red regions, i.e. for $t \approx \tau$. Transient diagrams \tilde{P} versus θ are shown for different values of \tilde{v}_c and for $\phi = 30^\circ$ (f) and $\phi = 45^\circ$ (g). Blue and red curves represent the starting condition and the steady-state limit, respectively. Black arrows indicate the time evolution of the process. figure.caption.10c showing θ_0 increasing with \tilde{P}_0 and \tilde{P}_0 increasing with \tilde{v}_c , respectively. Following Eq. (1equation.2.1), once the peeling starts, the value of $\theta(t)$ depends on the interplay between (i) the peeling front propagation, causing a linear increase of s_d , and (ii) the detached tape relaxation, increasing the term ΔL . For $\tilde{t} \ll 1$, a rough estimation of $\dot{\theta}$ can be derived from Eq. (1equation.2.1) as $\dot{\theta} \propto d(\Delta L)/dt - \beta v_c$, with $\beta = \beta(\theta_0)$ being a monotonically increasing function; indeed, in agreement with Fig. 3Top row: the initial \tilde{P}_0 and long-term \tilde{P}_S dimensionless peeling force as functions of the dimensionless adhesion energy $\tilde{\gamma}_0$ (a), the viscoelastic parameter $\kappa = E_\infty/E_0$ (b), and the dimensionless peeling front velocity \tilde{v}_c (c). In figure (c), the rate-dependent dimensionless adhesion energy $\tilde{\gamma}$ is also shown for comparison (dashed line). Notably, $\kappa = 1$ corresponds to elastic tapes. Bottom row: the time-history of the normalized peeling force \tilde{P}/\tilde{P}_S (d) and peeling angle θ (e) for different values of the dimensionless peeling front velocity \tilde{v}_c and initial undeformed configurations. Non-monotonic behavior occurs in the red regions, i.e. for $t \approx \tau$. Transient diagrams \tilde{P} versus θ are shown for different values of \tilde{v}_c and for $\phi = 30^\circ$ (f) and $\phi = 45^\circ$ (g). Blue and red curves represent the starting condition and the steady-state limit, respectively. Black arrows indicate the time evolution of the process. figure.caption.10e, f, and g, the peeling angle θ at $\tilde{t} \ll 1$ can either decrease (at high velocity, i.e. $\tilde{v}_c \approx 1000$) or increase (at low velocity, i.e. $\tilde{v}_c \approx 10$), while in the long-term limit $\theta(\tilde{t} \gg 1) \approx \theta_S$ eventually leading to non-monotonic behavior, depending on the specific value of θ_S . The normalized peeling force \tilde{P}/\tilde{P}_S in Fig. 3Top row: the initial \tilde{P}_0 and long-term \tilde{P}_S dimensionless peeling force as functions of the dimensionless adhesion energy $\tilde{\gamma}_0$ (a), the viscoelastic parameter $\kappa = E_\infty/E_0$ (b), and the dimensionless peeling front velocity \tilde{v}_c (c). In figure (c), the rate-dependent dimensionless adhesion energy $\tilde{\gamma}$ is also shown for comparison (dashed line). Notably, $\kappa = 1$ corresponds to elastic tapes. Bottom row: the time-history of the normalized peeling force \tilde{P}/\tilde{P}_S (d) and peeling angle θ (e) for different values of the dimensionless peeling front velocity \tilde{v}_c and initial undeformed configurations. Non-monotonic behavior occurs in the red regions, i.e. for $t \approx \tau$. Transient diagrams \tilde{P} versus θ are shown for different values of \tilde{v}_c and for $\phi = 30^\circ$ (f) and $\phi = 45^\circ$ (g). Blue and red curves represent the starting condition and the steady-state limit, respectively. Black arrows indicate the time evolution of the process. figure.caption.10d, f, and g is non-monotonic, as

well, since high values of θ lead to low values of \tilde{P}/\tilde{P}_S and vice versa, as expected [34, 54, 76].

3.2. Constant peeling force

In this section, we investigate the viscoelastic V peeling behavior under a constant peeling force P , such as under the action of a dead weight. Surprisingly, the results show that the peeling process can either start and indefinitely propagate, start and then stop after some time, or not even start at all, depending on the value of P and initial tape geometry (i.e., the undeformed angle ϕ and length L_i). The boundaries between these qualitatively different behaviors depend on the peeling front velocity, which is not known *a priori* in this case; therefore, the critical (minimum) forces for peeling start and steady-state propagation must be sought for both $v_c \gg d/\tau$ and $v_c \ll d/\tau$ assuming $\gamma \approx \gamma_0$, as for real thin tapes $\tilde{v}_\gamma \approx 10d/\tau$. As discussed at the end of Section 2, in the former case, critical loads for peeling start P_1 and steady-state propagation P_2 are given by Eqs. (14equation.3.14, 15equation.3.15) and Eqs. (11equation.2.11, 12equation.2.12), respectively, with $\gamma \approx \gamma_0$. On the contrary, in the latter case (i.e., for $v_c \ll d/\tau$), the critical forces P_3 (start) and P_4 (steady-state propagation) are given by the same equations with the high-frequency modulus E_∞ replaced by the low-frequency one E_0 and, again, with $\gamma \approx \gamma_0$.

The map in Fig. 4(a) The initial $[\tilde{v}_c]_0$ and long-term $[\tilde{v}_c]_S$ dimensionless peeling front velocity as functions of the dimensionless peeling force \tilde{P} . (b) The time-history of the normalized peeling front velocity $\tilde{v}_c/[\tilde{v}_c]_0$ for different values of dimensionless peeling force \tilde{P} . (c) The state map of the possible peeling behavior as a function of the dimensionless applied peeling force \tilde{P} and undeformed tape angle ϕ . \tilde{P}_1 and \tilde{P}_2 are the critical (minimum) force for peeling start and steady-state propagation calculated with $v_c \gg d/\tau$, while \tilde{P}_3 and \tilde{P}_4 refer to the same critical conditions when $v_c \ll d/\tau$ (further know are given in the text). Results refer to $\kappa = 10$ and $\tilde{\gamma}_0 = 0.02$. figure.caption.12c shows the possible peeling behaviors as discussed above as functions of the dimensionless applied peeling force \tilde{P} and undeformed tape angle ϕ (we assume $L_i = 100d$ for all calculations). Specifically, in region I the peeling does not propagate, in region II-III the peeling propagation starts and then stops after some time, and in regions IV-V-VI-VII the peeling propagates indefinitely approaching the steady-state regime (though in IV and V the long-term velocity is lower than d/τ). The present model predictions are rigorously valid in regions I and VII; nonetheless, qualitative insight can also be inferred for regions III and V, as a steady-state propagation with very low velocity (about $d/\tau \approx 10^{-4}$ m/s) qualitatively corresponds to a peeling stop (i.e., as in case III), for region VI, where $v_c \approx d/\tau$ when peeling starts and then rapidly increases, and for region II, as the peeling cannot be sustained in steady-state conditions regardless of the starting behavior. Finally, region IV cannot be accounted for in the present framework, as the specific viscoelastic behavior close to the peeling front does really matter throughout the whole process evolution. In most cases, real systems belong to the first scenario, with $v_c \gg d/\tau$.

The peeling front velocity calculated at the process start $[v_c]_0$ and in the long-term steady-state $[v_c]_S$ limit are shown in Fig. 4(a) The initial $[\tilde{v}_c]_0$ and long-term $[\tilde{v}_c]_S$ dimensionless peeling front velocity as functions of the dimensionless peeling force \tilde{P} . (b) The time-history of the normalized peeling front velocity $\tilde{v}_c/[\tilde{v}_c]_0$ for different values of dimensionless peeling force \tilde{P} . (c) The state map of the possible peeling behavior as a function of the dimensionless applied peeling force \tilde{P} and undeformed tape angle ϕ . \tilde{P}_1 and \tilde{P}_2 are the critical (minimum) force for peeling start and steady-state propagation calculated with $v_c \gg d/\tau$, while \tilde{P}_3

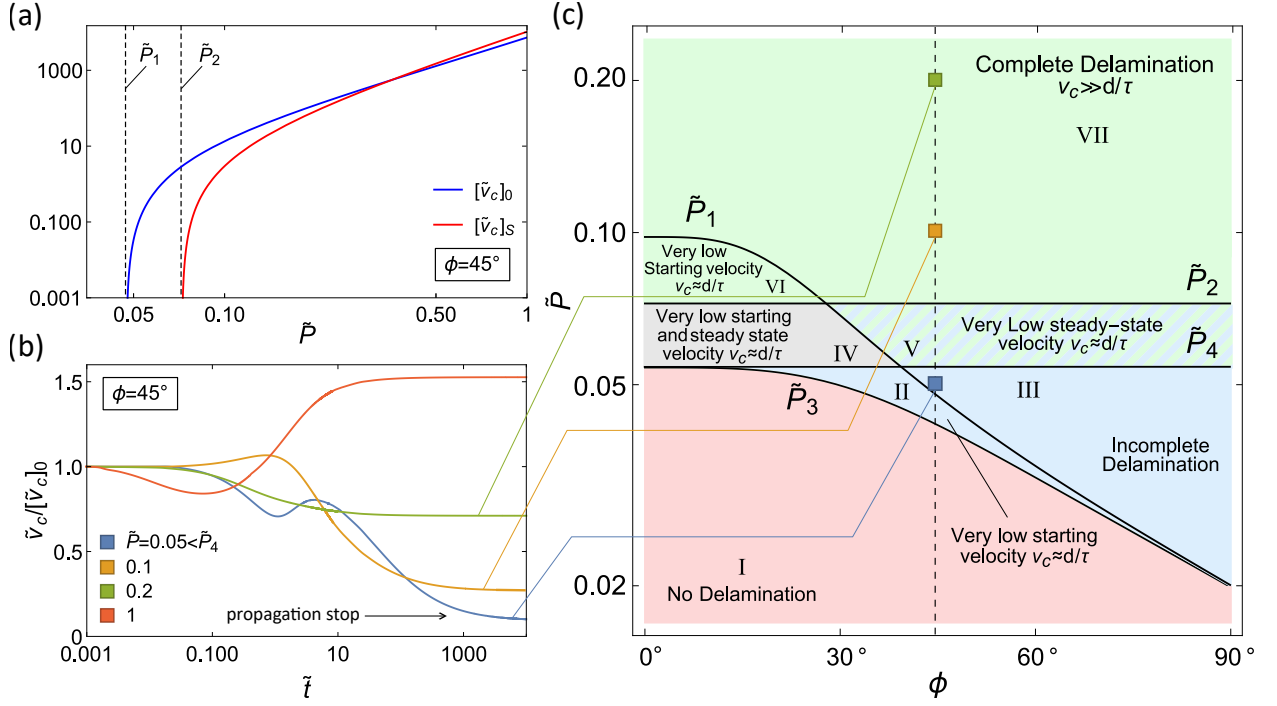


FIG. 4: (a) The initial $[\tilde{v}_c]_0$ and long-term $[\tilde{v}_c]_s$ dimensionless peeling front velocity as functions of the dimensionless peeling force \tilde{P} . (b) The time-history of the normalized peeling front velocity $\tilde{v}_c/[\tilde{v}_c]_0$ for different values of dimensionless peeling force \tilde{P} . (c) The state map of the possible peeling behavior as a function of the dimensionless applied peeling force \tilde{P} and undeformed tape angle ϕ . \tilde{P}_1 and \tilde{P}_2 are the critical (minimum) force for peeling start and steady-state propagation calculated with $v_c \gg d/\tau$, while \tilde{P}_3 and \tilde{P}_4 refer to the same critical conditions when $v_c \ll d/\tau$ (further know are given in the text). Results refer to $\kappa = 10$ and $\tilde{\gamma}_0 = 0.02$.

and \tilde{P}_4 refer to the same critical conditions when $v_c \ll d/\tau$ (further know are given in the text). Results refer to $\kappa = 10$ and $\tilde{\gamma}_0 = 0.02$. figure.caption.12a as functions of \tilde{P} . More interestingly, two different peeling behaviors are shown in Fig. 4(a) The initial $[\tilde{v}_c]_0$ and long-term $[\tilde{v}_c]_s$ dimensionless peeling front velocity as functions of the dimensionless peeling force \tilde{P} . (b) The time-history of the normalized peeling front velocity $\tilde{v}_c/[\tilde{v}_c]_0$ for different values of dimensionless peeling force \tilde{P} . (c) The state map of the possible peeling behavior as a function of the dimensionless applied peeling force \tilde{P} and undeformed tape angle ϕ . \tilde{P}_1 and \tilde{P}_2 are the critical (minimum) force for peeling start and steady-state propagation calculated with $v_c \gg d/\tau$, while \tilde{P}_3 and \tilde{P}_4 refer to the same critical conditions when $v_c \ll d/\tau$ (further know are given in the text). Results refer to $\kappa = 10$ and $\tilde{\gamma}_0 = 0.02$. figure.caption.12b, with respect to the time-history of the normalized peeling front velocity $\tilde{v}_c/[\tilde{v}_c]_0$ for different values of \tilde{P} belonging to regions VII and III. In the latter case (blue curve), for $\tilde{P} < \tilde{P}_4$, the peeling front velocity decreases down to full stop. In the other cases, all belonging to region VII, after the initial non-monotonic behavior, in the long-term a steady-state behavior is approached, with endless propagation occurring at velocity $[v_c]_s$.

3.3. Constant pulling velocity

The final case we deal with is with the tape being pulled at a constant velocity \tilde{v}_P . In this case, the start of peeling propagation does not coincide with the application of the pulling velocity. Indeed, before peeling starts, the stress σ in the non-adhering tape must increase from zero to a certain critical value σ_{cr} . The energy-based procedure to calculate such a critical condition is given in Appendix B section*.19.

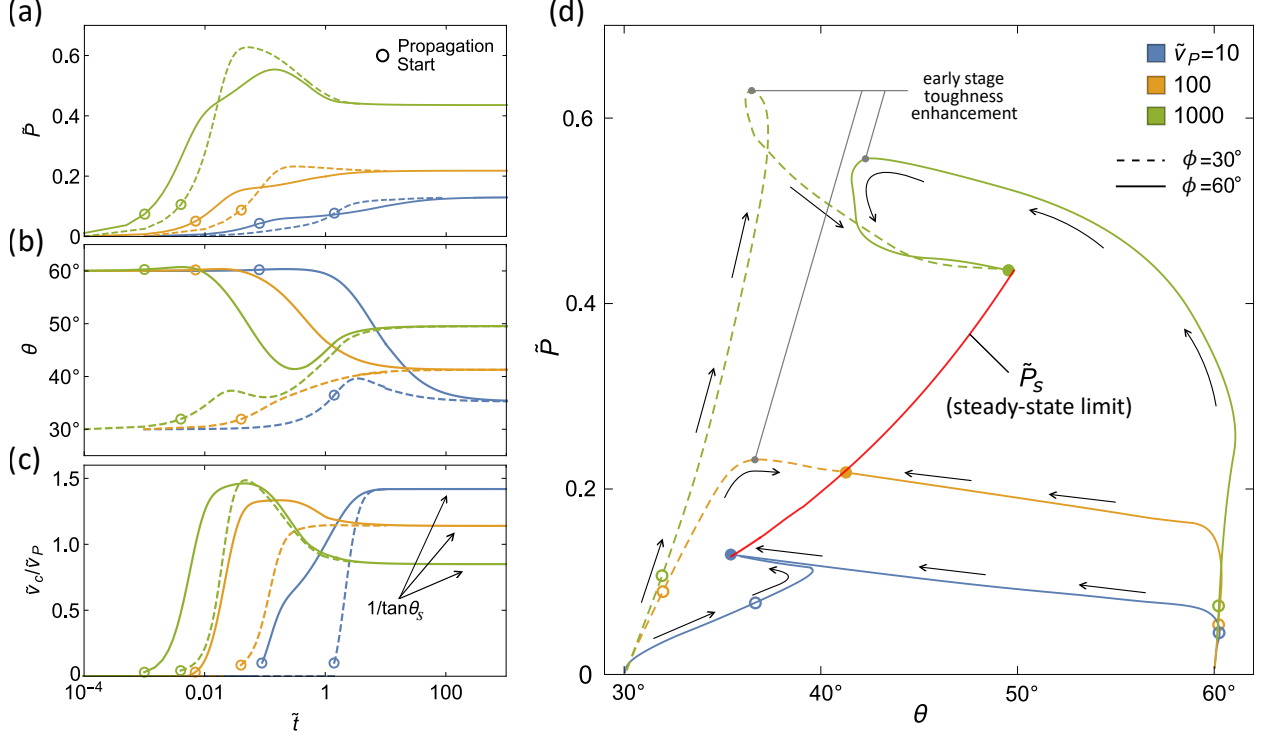


FIG. 5: The time-history of the dimensionless peeling force \tilde{P} (a), the peeling angle θ (c), and the peeling velocity ratio \tilde{v}_c/\tilde{v}_P (c), together with the transient diagram \tilde{P} vs. θ (d) for different values of the dimensionless pulling velocity \tilde{v}_P . Two undeformed tape angles are considered. The circles indicate the instant when peeling front propagation starts. The red curve in (d) represents the steady-state peeling limit, and black arrows indicate the time evolution of the process. Results refer to $\kappa = 10$ and $\tilde{\gamma}_0 = 0.02$.

In Figs. 5The time-history of the dimensionless peeling force \tilde{P} (a), the peeling angle θ (c), and the peeling velocity ratio \tilde{v}_c/\tilde{v}_P (c), together with the transient diagram \tilde{P} vs. θ (d) for different values of the dimensionless pulling velocity \tilde{v}_P . Two undeformed tape angles are considered. The circles indicate the instant when peeling front propagation starts. The red curve in (d) represents the steady-state peeling limit, and black arrows indicate the time evolution of the process. Results refer to $\kappa = 10$ and $\tilde{\gamma}_0 = 0.02$.figure.caption.14a, b, and c, we show, respectively, the time-history of \tilde{P} , θ and \tilde{v}_c/\tilde{v}_P , for different values of the dimensionless pulling velocity \tilde{v}_P and undeformed angle ϕ . Circles indicate the peeling start, which increases with ϕ reducing, as expected from Eq. (B1equation.B.1). In the long-term limit, steady-state propagation occurs, with $[v_c]_S/\tilde{v}_P = 1/\tan\theta_S$ according to Eq. (13equation.2.13). The most interesting result from Fig. 5The time-history of the

dimensionless peeling force \tilde{P} (a), the peeling angle θ (c), and the peeling velocity ratio \tilde{v}_c/\tilde{v}_P (c), together with the transient diagram \tilde{P} vs. θ (d) for different values of the dimensionless pulling velocity \tilde{v}_P . Two undeformed tape angles are considered. The circles indicate the instant when peeling front propagation starts. The red curve in (d) represents the steady-state peeling limit, and black arrows indicate the time evolution of the process. Results refer to $\kappa = 10$ and $\tilde{\gamma}_0 = 0.02$. figure.caption.14a, is that the peeling force \tilde{P} may present a maximum at the early stage, right after the peeling start, at a relatively high pulling velocity \tilde{v}_P . This is also shown in Fig. 5. The time-history of the dimensionless peeling force \tilde{P} (a), the peeling angle θ (c), and the peeling velocity ratio \tilde{v}_c/\tilde{v}_P (c), together with the transient diagram \tilde{P} vs. θ (d) for different values of the dimensionless pulling velocity \tilde{v}_P . Two undeformed tape angles are considered. The circles indicate the instant when peeling front propagation starts. The red curve in (d) represents the steady-state peeling limit, and black arrows indicate the time evolution of the process. Results refer to $\kappa = 10$ and $\tilde{\gamma}_0 = 0.02$. figure.caption.14d, clearly indicating that this is associated with a temporary reduction of the peeling angle θ which results from a fast increase of v_c before viscoelastic relaxation occurs (i.e., for $\tilde{t} \ll 1$). Such a peculiar feature may partially link to the superior adhesive performance of V-shaped natural systems, such as spider webs [48] and mussels byssus [49], under the action of high-speed (impact) loading conditions. In the latter case, for instance, Cohen et Al. [78] have shown that the single byssus is highly stretchable, due to the heterogeneous filament structure (a system of nonlinear swollen springs); here, we suggest that also the interplay between byssus rheology and V-shaped multiple threads geometry (see Fig. 1. Examples of V-peeling configurations in natural systems and practical applications: (a) spider web anchors (from Ref. [66]); (b) gecko upside down climbing (adapted from Wikipedia); (c) mussel byssus threads (from Wikipedia); (d) loop tack test schematic (from Ref. [51]). figure.caption.4c) may contribute to the observed tougher adhesive response under dynamic loads [49].

4. CONCLUSIONS

In this study, we model the peeling behavior of a viscoelastic thin tape arranged in V-shaped peeling configuration. Specifically, the velocity-dependent condition for peeling front propagation is found in terms of energy balance between the work per unit time done by the internal stress in the tape, the external forces acting on the system, and the surface adhesion forces. An *ad hoc* numerical procedure is derived to predict the time-evolution of the peeling process, taking into account the time-varying viscoelastic relaxation of the detached tape. We consider three possible physical scenarios for peeling propagation: constant peeling front velocity, constant peeling force, and constant pulling velocity at the tape tip.

In the long-term limit, the peeling propagation asymptotically approaches a steady-state elastic-like behavior, regardless of the specific controlled parameter. However, the initial transient peeling behavior is strongly affected by the tape viscoelasticity and undeformed geometry, and presents non-monotonic time evolution of the peeling force and angle. More in detail, when a constant force is applied, we found that the peeling can either endlessly propagate, start and stop after some time, or not even start. Which of these scenarios occurs seems to depend only on the applied force value and undeformed non-adhering tape geometry (angle and length).

More surprisingly, when the pulling velocity at the tape tip is assigned, as in the case of impact loads acting on an attached object, the peeling propagation is delayed against

the instant of force application, and the force required to sustain the peeling propagation (i.e., the peeling toughness) can be temporarily larger than in stationary conditions. This mechanism might be qualitatively related to the high-speed superior adhesive performance observed in several natural systems.

ACKNOWLEDGMENTS

This work was partly supported by the Italian Ministry of Education, University and Research under the Programme “Department of Excellence” Legge 232/2016” and partly by the European Union - NextGenerationEU (National Sustainable Mobility Center CN000000023, Italian Ministry of University and Research Decree n. 1033 - 17/06/2022, Spoke 11 - Innovative Materials & Lightweighting). The opinions expressed are those of the authors only and should not be considered as representative of the European Union or the European Commission’s official position. Neither the European Union nor the European Commission can be held responsible for them.

Appendix A: Numerical calculation of peeling process evolution

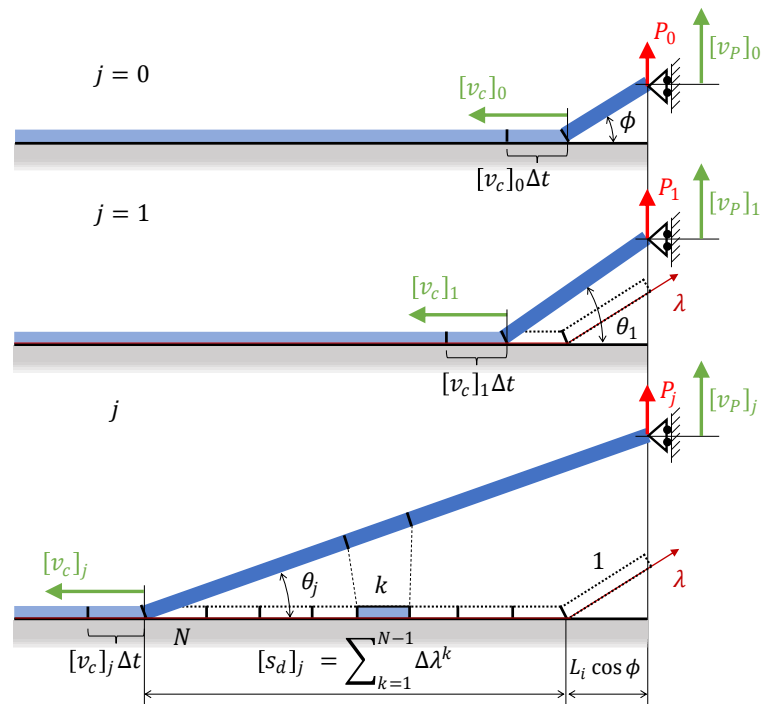


FIG. A.1: Scheme of the tape discretization: at the generic j -th time instant, the tape mesh is updated by including a freshly detached element of undeformed length $\Delta\lambda = [v_c]_j \Delta t$.

The process evolution can be calculated by numerical integration of Eqs. (2equation.2.2, 1equation.2.1). However, dealing with a viscoelastic tape, the governing equations depend on the entire time-history of the process and the solution of Eqs. (2equation.2.2, 1equation.2.1)

must be iteratively sought by successively updating the system configurations as the peeling front moves.

The numerical method is based on uniform time discretization, with time step $\Delta t \ll \tau$, and non-uniform tape mesh. In the following discussion, the notation η_j^k represents the discrete value of the generic quantity η at the j -th time instant in the k -th tape element. Only the non-adhering tape is discretized, and the mesh is updated at each time step so that, at the generic time $t_j = j\Delta t$, an element of (undeformed) length $\Delta\lambda = [v_c]_j \Delta t$ is added to the mesh due to peeling front motion. The resulting non-uniform "incremental" mesh has two primary advantages: (i) the total number of elements does not need to be fixed a priori; (ii) only the non-adhering tape is discretized, and the computational cost is reduced. More in detail, referring to Fig. (A.1 Scheme of the tape discretization: at the generic j -th time instant, the tape mesh is updated by including a freshly detached element of undeformed length $\Delta\lambda = [v_c]_j \Delta t$. figure.caption.18), $N_j = j + 1$ is the total number of tape elements at the j -th time instant, with the first element $\Delta\lambda^1$ being the initial non-adhering tape (i.e., $\Delta\lambda^1 = L_i$) and the N -th element $\Delta\lambda^{N_j}$ being last detached element ($\Delta\lambda^{N_j} = \Delta t [v_c]_{j-1}$). Therefore, the detached tape projection s_j is given by

$$s_j = L_i \cos \phi + [s_d]_j = L_i \cos \phi + \sum_{k=2}^{N_j} \Delta\lambda^k. \quad (\text{A1})$$

The discrete form of Eqs. (9equation.2.9, 7equation.2.7) is

$$[W_{ad}]_j = -[v_c \gamma]_j w \quad (\text{A2})$$

$$[W_P]_j = A_t [v_P \sigma]_j \sin \theta_j \quad (\text{A3})$$

where, from Eq. (8equation.2.8),

$$[v_P]_j = [v_c]_j \tan \theta_j + \frac{s_j}{\cos^2 \theta_j} \frac{\theta_j - \theta_{j-1}}{\Delta t}. \quad (\text{A4})$$

Integrating by parts, Eq. (5equation.2.5) is rewritten as

$$\varepsilon(\lambda, t) = \frac{\sigma(\lambda, t)}{E_\infty} + \int_{-\infty}^t \dot{\mathcal{J}}(t - t') \sigma(\lambda, t') dt', \quad (\text{A5})$$

where we used $\mathcal{J}(0) = E_\infty^{-1}$, and $\sigma(\lambda, -\infty) = 0$; the discrete form of Eq. (A5equation.A.5) gives the elongation of the generic k -th element of the non-adhering tape at the j -th time instant as

$$\varepsilon_j^k = \frac{\sigma_j^k}{E_\infty} + \Delta t \sum_{h=0}^j \dot{\mathcal{J}}_{j-h} \sigma_h, \quad (\text{A6})$$

with $\sigma_j^k = \sigma_j = P_j / (A_t \sin \theta_j)$ for all the tape elements.

To calculate W_{in} , we observe that the term $\partial \varepsilon / \partial t(\lambda, t)$ diverges at the peeling front (i.e., for $\lambda \rightarrow \lambda_c(t)$), as we assume a step-change in the tape stress σ . In this case, the discretized form of Eq. (3equation.2.3) can be conveniently rewritten as

$$\frac{[W_{in}]_j}{A_t} = -\sigma_j \dot{\varepsilon}_j^N \Delta\lambda^N - \sigma_j \sum_{k=1}^{N-1} \dot{\varepsilon}_j^k \Delta\lambda^k, \quad (\text{A7})$$

where, according to [54, 79], since $v_c \gg d/\tau$, the first right-hand side term can be calculated as

$$\sigma_j \dot{\varepsilon}_j^N \Delta \lambda^N = \frac{[\sigma^2 v_c]_j}{2E_\infty}. \quad (\text{A8})$$

Combining Eqs. (A7equation.A.7, A8equation.A.8), the discretized form of Eq. (3equation.2.3) is

$$\frac{[W_{in}]_j}{A_t} = -\frac{[v_c \sigma^2]_j}{2E_\infty} - \sigma_j \sum_{k=1}^{N-1} \left[\frac{\varepsilon_j - \varepsilon_{j-1}}{\Delta t} \Delta \lambda \right]^k \quad (\text{A9})$$

Finally, using Eqs. (A2equation.A.2, A3equation.A.3, A9equation.A.9) in Eq. (2equation.2.2) gives the discrete form for the instantaneous energy balance equation

$$[W_P]_j + [W_{in}]_j + [W_{ad}]_j = 0 \quad (\text{A10})$$

and, from Eq. (1equation.2.1) we have

$$\frac{s_j}{\cos \theta_j} = \sum_{k=1}^N (1 + \varepsilon_j^k) \Delta \lambda^k, \quad (\text{A11})$$

where $(1 + \varepsilon_j^k) \Delta \lambda^k$ is the deformed length of the generic k -th element at the j -th time instant. The process time evolution is obtained from an iterative algorithm based on the Newton-Rapshon method that solves Eqs. (A10equation.A.10, A11equation.A.11) for the unknown peeling quantities at each time instant.

Appendix B: Starting condition under constant pulling velocity

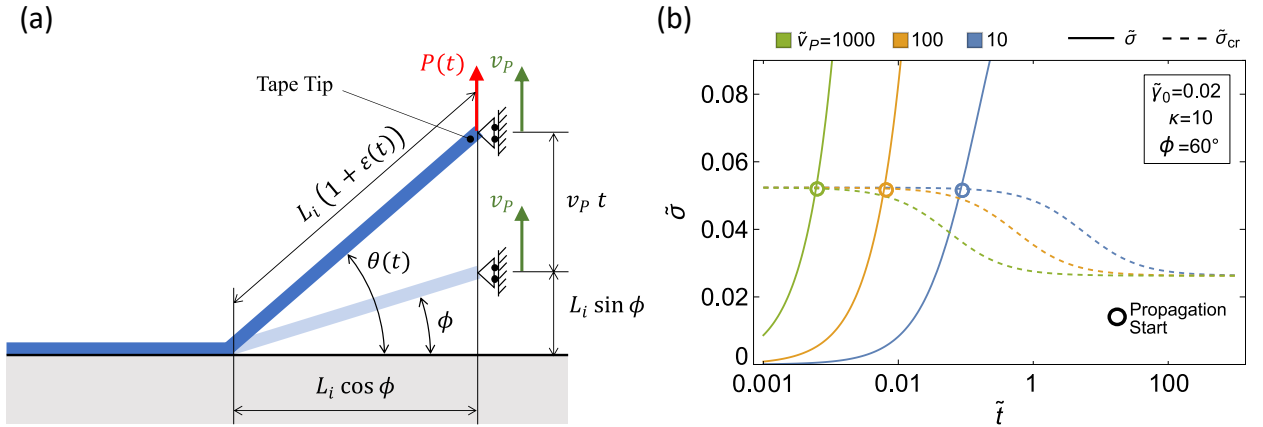


FIG. B.1: (a) A schematic of the tape in undeformed condition, and at a generic time $t < t^*$, i.e. before the peeling propagation starts. (b) The dimensionless stress $\tilde{\sigma}$ in the tape (solid curves) and the dimensionless critical stress $\tilde{\sigma}_{cr}$ required to start the peeling propagation (dashed curves) as functions of the dimensionless time \tilde{t} for different dimensionless tape tip velocity \tilde{v}_p . Circles indicate the instant of propagation start.

We consider that at time $t = 0$ the tape tip is pulled at a constant velocity v_P . In this case, the deformation $\varepsilon(t)$ and stress $\sigma(t)$ in the non-adhering tape monotonically increase, and peeling front propagation starts at time t^* when $\sigma(t^*) = \sigma_{cr}(t^*)$. The value σ_{cr} depends on the energy balance

$$\frac{\sigma_{cr}^2}{2E_\infty} + \sigma_{cr}[1 - \cos \theta] = \frac{\gamma_0}{d}, \quad (\text{B1})$$

where we assumed that $v_c(t^*) \ll v_\gamma$.

According to Fig. B.1(a) A schematic of the tape in undeformed condition, and at a generic time $t < t^*$, i.e. before the peeling propagation starts. (b) The dimensionless stress $\tilde{\sigma}$ in the tape (solid curves) and the dimensionless critical stress $\tilde{\sigma}_{cr}$ required to start the peeling propagation (dashed curves) as functions of the dimensionless time \tilde{t} for different dimensionless tape tip velocity \tilde{v}_P . Circles indicate the instant of propagation start. figure.caption.20a, before peeling front propagation (i.e., for $t < t^*$), the peeling angle is given by

$$\tan \theta = \frac{L_i \sin \phi + v_P t}{L_i \cos \phi}, \quad (\text{B2})$$

where $v_P t$ is the tape tip vertical displacement at the generic time t . Similarly, since $L_i + \Delta L = L_i \cos \phi / \cos \theta$ is the deformed tape length, the tape uniform deformation before peeling propagation is

$$\varepsilon(t) = \frac{L_i + \Delta L}{L_i} - 1 = \frac{\cos \phi}{\cos \theta} - 1. \quad (\text{B3})$$

Finally, using the viscoelastic constitutive equation, we can calculate the uniform stress in the detached tape as

$$\sigma(t) = \int_{-\infty}^t \mathcal{R}(t - t') \dot{\varepsilon}(t') dt', \quad (\text{B4})$$

where \mathcal{R} is the stress-relaxation function given by

$$\mathcal{R}(t) = E_0 + (E_\infty - E_0)e^{t/\tau_r}, \quad (\text{B5})$$

with $\tau_r = \tau/(1 + \Delta)$ being the relaxation time, and $\Delta = E_\infty/E_0 - 1$ being the relaxation strength.

The peeling starting condition $\sigma(t^*) = \sigma_{cr}(t^*)$ is then obtained by simultaneously solving Eqs. (B1equation.B.1-B4equation.B.4). In Figure B.1(a) A schematic of the tape in undeformed condition, and at a generic time $t < t^*$, i.e. before the peeling propagation starts. (b) The dimensionless stress $\tilde{\sigma}$ in the tape (solid curves) and the dimensionless critical stress $\tilde{\sigma}_{cr}$ required to start the peeling propagation (dashed curves) as functions of the dimensionless time \tilde{t} for different dimensionless tape tip velocity \tilde{v}_P . Circles indicate the instant of propagation start. figure.caption.20b we show the time-history of $\tilde{\sigma}(t)$ and $\tilde{\sigma}_{cr}(t)$, for different dimensionless pulling velocities \tilde{v}_P . Increasing \tilde{v}_P leads to faster stress increase in the viscoelastic tape, thus peeling propagation starts sooner.

Once the peeling front propagation starts, the numerical algorithm described in Appendix Asection*.17 can be used to calculate the time evolution of the peeling process, with t^* corresponding to $j = 0$. In the present formalism, the peeling front velocity $v_c(t^*)$ at the instant of the peeling propagation start cannot be exactly determined; however, in the reasonable assumption for practical applications that $v_P / \tan \theta_S = [v_c]_S \gg d/\tau$, the system

rapidly approaches the conditions $v_c > d/\tau$ at the very early stage of peeling propagation. As a consequence, we set $\tilde{v}_c(t^*) \approx 1$.

-
- [1] Creton, C., Gorb, S., 2007. Sticky feet: from animals to materials. *Mrs Bulletin*, 32(6), 466-472.
 - [2] Cho, K. J., Koh, J. S., Kim, S., Chu, W. S., Hong, Y., Ahn, S. H., 2009. Review of manufacturing processes for soft biomimetic robots. *International Journal of Precision Engineering and Manufacturing*, 10(3), 171-181.
 - [3] Min, W. L., Jiang, B., Jiang, P., 2008. Bioinspired self-cleaning antireflection coatings. *Advanced Materials*, 20(20), 3914-3918.
 - [4] Meitl, M. A., Zhu, Z. T., Kumar, V., Lee, K. J., Feng, X., Huang, Y. Y., ... , Rogers, J. A., 2006. Transfer printing by kinetic control of adhesion to an elastomeric stamp. *Nature materials*, 5(1), 33-38.
 - [5] Hwang, J., Jeong, Y., Park, J. M., Lee, K. H., Hong, J. W., Choi, J., 2015. Biomimetics: forecasting the future of science, engineering, and medicine. *International journal of nanomedicine*, 10, 5701.
 - [6] Shafiee, A., Cavalcanti, A. S., Saidy, N. T., Schneidereit, D., Friedrich, O., Ravichandran, A., ..., Hutmacher, D. W., 2021. Convergence of 3D printed biomimetic wound dressings and adult stem cell therapy. *Biomaterials*, 268, 120558.
 - [7] Cacucciolo, V., Shea, H., Carbone, G., 2021. Peeling in electroadhesion soft grippers. *Extreme Mechanics Letters*, 101529.
 - [8] Hawkes, E. W., Jiang, H., Christensen, D. L., Han, A. K., Cutkosky, M. R., 2017. Grasping without squeezing: Design and modeling of shear-activated grippers. *IEEE Transactions on Robotics*, 34(2), 303-316.
 - [9] Kwak, M. K., Jeong, H. E., Suh, K. Y., 2011. Rational design and enhanced biocompatibility of a dry adhesive medical skin patch. *Advanced Materials*, 23(34), 3949-3953.
 - [10] W. G. Bae, D. Kim, M. K. Kwak, L. Ha, S. M. Kang, K. Y. Suh, 2013. Enhanced skin adhesive patch with modulus-tunable composite micropillars, *Advanced healthcare materials* 2 (1) 109–113.
 - [11] R. H. Plaut, 2010. Two-dimensional analysis of peeling adhesive tape from human skin, *The Journal of Adhesion* 86 (11) 1086–1110.
 - [12] A. Karwoski, R. Plaut, 2004. Experiments on peeling adhesive tapes from human forearms, *Skin Research and Technology* 10 (4) 271–277.
 - [13] M. Sexsmith, T. Troczynski, 1994. Peel adhesion test for thermal spray coatings, *Journal of Thermal Spray Technology* 3 404–411.
 - [14] Wang, Lei, and Jing Liu, 2019. "Advances in the development of liquid metal-based printed electronic inks." *Frontiers in materials* 6: 303.
 - [15] X. Feng, M. A. Meitl, A. M. Bowen, Y. Huang, R. G. Nuzzo, J. A. Rogers, 2007. Competing fracture in kinetically controlled transfer printing, *Langmuir* 23 (25) 12555–12560.
 - [16] Song, S., Sitti, M., 2014. Soft grippers using micro-fibrillar adhesives for transfer printing. *Advanced Materials*, 26(28), 4901-4906.
 - [17] Sato, N., Murata, A., Fujie, T., Takeoka, S., 2016. Stretchable, adhesive and ultra-

- conformable elastomer thin films. *Soft Matter*, 12(45), 9202-9209.
- [18] Rivlin, R. S., 1997. The effective work of adhesion. In *Collected papers of RS Rivlin* (pp. 2611-2614). Springer, New York, NY.
 - [19] Eremeyev, V. A., Naumenko, K., 2015. A relationship between effective work of adhesion and peel force for thin hyperelastic films undergoing large deformation. *Mechanics Research Communications*, 69, 24-26.
 - [20] Molinari, A., Ravichandran, G., 2008. Peeling of elastic tapes: effects of large deformations, pre-straining, and of a peel-zone model. *The Journal of Adhesion*, 84(12), 961-995.
 - [21] Williams, J. A., Kauzlarich, J. J., 2004. Peeling shear and cleavage failure due to tape prestrain. *The journal of Adhesion*, 80(5), 433-458.
 - [22] Chen, B., Wu, P., Gao, H., 2009. Pre-tension generates strongly reversible adhesion of a spatula pad on substrate. *Journal of the Royal Society Interface*, 6(35), 529-537.
 - [23] Putignano, C., Afferrante, L., Carbone, G., Demelio, G., 2014. Double peeling of elastic pre-tensioned tapes. *Frattura ed Integrità Strutturale*, 8(30), 237-243.
 - [24] Z. Peng, S. Chen, 2015. Effect of bending stiffness on the peeling behavior of an elastic thin film on a rigid substrate, *Physical Review E* 91 (4) 042401.
 - [25] R. A. Sauer, 2011. The peeling behavior of thin films with finite bending stiffness and the implications on gecko adhesion, *The Journal of Adhesion* 87 (7-8) 624-643.
 - [26] Kim, K. S., Kim, J., 1988. Elasto-plastic analysis of the peel test for thin film adhesion.
 - [27] Kovalchick, C., Molinari, A., Ravichandran, G., 2014. Rate dependent adhesion energy and nonsteady peeling of inextensible tapes. *Journal of Applied Mechanics*, 81(4).
 - [28] Maugis, D., Barquins, M., 1980. Fracture mechanics and adherence of viscoelastic solids. In *Adhesion and adsorption of polymers* (pp. 203-277). Springer, Boston, MA.
 - [29] Zhou, M., Tian, Y., Pesika, N., Zeng, H., Wan, J., Meng, Y., Wen, S., 2011. The extended peel zone model: effect of peeling velocity. *The Journal of Adhesion*, 87(11), 1045-1058.
 - [30] De, R., Maybhate, A., Ananthakrishna, G., 2004. Dynamics of stick-slip in peeling of an adhesive tape. *Physical Review E*, 70(4), 046223.
 - [31] M.-J. Dalbe, P.-P. Cortet, M. Ciccotti, L. Vanel, S. Santucci, 2015. Multiscale stick-slip dynamics of adhesive tape peeling, *Physical review letters* 115 (12) 128301.
 - [32] Camara, C. G., Escobar, J. V., Hird, J. R., Putterman, S. J., 2008. Correlation between nanosecond X-ray flashes and stick-slip friction in peeling tape. *nature*, 455(7216), 1089-1092.
 - [33] Begley, M.R., Collino, R.R., Israelachvili, J.N., McMeeking, R.M., 2013. Peeling of a tape with large deformations and frictional sliding. *J. Mech. Phys. Solids* 61(5), 1265-1279
 - [34] Kendall, K., 1971. The adhesion and surface energy of elastic solids. *Journal of Physics D: Applied Physics*, 4(8), 1186.
 - [35] Pelfrene, J., Van Dam, S., Van Paepegem, W., 2015. Numerical analysis of the peel test for characterisation of interfacial debonding in laminated glass. *International Journal of Adhesion and Adhesives*, 62, 146-153.
 - [36] Fafenrot, S., Korger, M., Ehrmann, A., 2019. Mechanical properties of composites

- from textiles and three-dimensional printed materials. In *Mechanical and Physical Testing of Biocomposites, Fibre-Reinforced Composites and Hybrid Composites* (pp. 409-425). Woodhead Publishing.
- [37] Menga, N., 2019. Rough frictional contact of elastic thin layers: The effect of geometrical coupling. *International Journal of Solids and Structures*, 164, 212-220.
 - [38] Menga, N., Carbone, G., Dini, D., 2021. Exploring the effect of geometric coupling on friction and energy dissipation in rough contacts of elastic and viscoelastic coatings. *Journal of the Mechanics and Physics of Solids*, 148, 104273.
 - [39] Müller, C., Müser, M. H., Carbone, G., Menga, N., 2023. Significance of Elastic Coupling for Stresses and Leakage in Frictional Contacts. *Physical Review Letters*, 131(15), 156201.
 - [40] Afferrante, L., Putignano, C., Menga, N., Carbone, G., 2019. Friction in rough contacts of linear viscoelastic surfaces with anisotropic statistical properties. *The European Physical Journal E*, 42, 1-8.
 - [41] Carbone, G., Mandriota, C., Menga, N., 2022. Theory of viscoelastic adhesion and friction. *Extreme Mechanics Letters*, 56, 101877.
 - [42] Shahsavani, H., Salili, S. M., Jáklí, A., Zhao, B., 2017. Thermally active liquid crystal network gripper mimicking the self-peeling of gecko toe pads. *Advanced Materials*, 29(3), 1604021.
 - [43] Heepe, L., Raguseo, S., Gorb, S. N., 2017. An experimental study of double-peeling mechanism inspired by biological adhesive systems. *Applied Physics A*, 123(2), 1-8.
 - [44] Pugno, N. M., 2011. The theory of multiple peeling. *International journal of fracture*, 171(2), 185-193.
 - [45] Bosia, F., Colella, S., Mattoli, V., Mazzolai, B., Pugno, N. M., 2014. Hierarchical multiple peeling simulations. *Rsc Advances*, 4(48), 25447-25452.
 - [46] Lepore, E., Pugno, F., Pugno, N. M., 2012. Optimal angles for maximal adhesion in living tokay geckos. *The Journal of Adhesion*, 88(10), 820-830.
 - [47] Gu, Z., Li, S., Zhang, F., Wang, S., 2016. Understanding surface adhesion in nature: a peeling model. *Advanced Science*, 3(7), 1500327.
 - [48] Cranford, S. W., Tarakanova, A., Pugno, N. M., Buehler, M. J., 2012. Nonlinear material behaviour of spider silk yields robust webs. *Nature*, 482(7383), 72-76.
 - [49] Qin, Z., Buehler, M. J., 2013. Impact tolerance in mussel thread networks by heterogeneous material distribution. *Nature communications*, 4(1), 1-8.
 - [50] Desmond, K. W., Zacchia, N. A., Waite, J. H., Valentine, M. T., 2015. Dynamics of mussel plaque detachment. *Soft matter*, 11(34), 6832-6839.
 - [51] Bartlett, M. D., Case, S. W., Kinloch, A. J., Dillard, D. A., 2023. Peel tests for quantifying adhesion and toughness: A review. *Progress in Materials Science*, 101086.
 - [52] Gent, A. N., Kaang, S., 1986. Pull-off forces for adhesive tapes. *Journal of applied polymer science*, 32(4), 4689-4700.
 - [53] Elder, T., Twohig, T., Singh, H., Croll, A. B., 2020. Adhesion of a tape loop. *Soft Matter*, 16(47), 10611-10619.
 - [54] Ceglie, M., Menga, N., Carbone, G., 2022. The role of interfacial friction on the peeling of thin viscoelastic tapes. *Journal of the Mechanics and Physics of Solids*, 159, 104706.
 - [55] Loukis, M. J., Aravas, N., 1991. The effects of viscoelasticity in the peeling of

- polymeric films. *The Journal of Adhesion*, 35(1), 7-22.
- [56] Chen, H., Feng, X., Huang, Y., Huang, Y., Rogers, J.A., 2013. Experiments and viscoelastic analysis of peel test with patterned strips for applications to transfer printing. *Journal of the Mechanics and Physics of Solids*, 61(8), 1737-1752.
 - [57] Benyahia, L., Verdier, C., Piau, J. M., 1997. The mechanisms of peeling of uncross-linked pressure sensitive adhesives. *The Journal of Adhesion*, 62(1-4), 45-73.
 - [58] Derail, C., Allal, A., Marin, G., Tordjeman, P., 1997. Relationship between viscoelastic and peeling properties of model adhesives. Part 1. Cohesive fracture. *The Journal of Adhesion*, 61(1-4), 123-157.
 - [59] Peng, Z., Wang, C., Chen, L., Chen, S., 2014. Peeling behavior of a viscoelastic thin-film on a rigid substrate. *International Journal of Solids and Structures*, 51(25-26), 4596-4603.
 - [60] Collino, R. R., Philips, N. R., Rossol, M. N., McMeeking, R. M., Begley, M. R., 2014. Detachment of compliant films adhered to stiff substrates via van der Waals interactions: role of frictional sliding during peeling. *Journal of The Royal Society Interface*, 11(97), 20140453.
 - [61] Zhu, Z., Xia, Y., Jiang, C., Yang, Z., Jiang, H., 2021. Investigation of zero-degree peeling behavior of visco-hyperelastic highly stretchable adhesive tape on rigid substrate. *Engineering Fracture Mechanics*, 241, 107368.
 - [62] Afferrante, L., Carbone, G., 2016. The ultratough peeling of elastic tapes from viscoelastic substrates. *Journal of the Mechanics and Physics of Solids*, 96, 223-234.
 - [63] Pierro, E., Afferrante, L., Carbone, G., 2020. On the peeling of elastic tapes from viscoelastic substrates: Designing materials for ultratough peeling. *Tribology International*, 146, 106060.
 - [64] Z. Zhu, Z. Yang, Y. Xia, H. Jiang, 2021. Controllable peeling of an elastic strip on a viscoelastic substrate, *Engineering Fracture Mechanics* 256, 107990.
 - [65] J. Renvoise, D. Burlot, G. Marin, C. Derail, 2009. Adherence performances of pressure sensitive adhesives on a model viscoelastic synthetic film: a tool for the understanding of adhesion on the human skin, *International journal of pharmaceutics* 368 (1-2) 83–88.
 - [66] Menga, N., Afferrante, L., Pugno, N. M., Carbone, G., 2018. The multiple V-shaped double peeling of elastic thin films from elastic soft substrates. *Journal of the Mechanics and Physics of Solids*, 113, 56-64.
 - [67] Menga, N., Dini, D., Carbone, G., 2020. Tuning the periodic V-peeling behavior of elastic tapes applied to thin compliant substrates. *International Journal of Mechanical Sciences*, 170, 105331.
 - [68] Lake, G. J., Stevenson, A., 1981. Wave phenomena in low angle peeling. *The Journal of Adhesion*, 12(1), 13-22.
 - [69] Maugis, D., Barquins, M., 1988. Stick-slip and peeling of adhesive tapes. In *Adhesion* 12 (pp. 205-222). Springer, Dordrecht.
 - [70] Cortet, P. P., Ciccotti, M., Vanel, L., 2007. Imaging the stick-slip peeling of an adhesive tape under a constant load. *Journal of Statistical Mechanics: Theory and Experiment*, 2007(03), P03005.
 - [71] Amouroux, N., Petit, J., Leger, L., 2001. Role of interfacial resistance to shear stress on adhesive peel strength. *Langmuir* 17, 6510–6517. doi:10. 1021/la010146r.

- [72] Ciccotti, M., Giorgini, B., Vallet, D., Barquins, M., 2004. Complex dynamics in the peeling of an adhesive tape. *International journal of adhesion and adhesives*, 24(2), 143-151.
- [73] He, L., Lou, J., Kitipornchai, S., Yang, J., Du, J., 2019. Peeling mechanics of hyperelastic beams: Bending effect. *International Journal of Solids and Structures*, 167, 184-191.
- [74] Gent, A. N., Hamed, G. R., 1977. Peel mechanics for an elastic-plastic adherend. *Journal of Applied Polymer Science*, 21(10), 2817-2831.
- [75] Marin, G., Derail, C., 2006. Rheology and adherence of pressure-sensitive adhesives. *The Journal of Adhesion*, 82(5), 469-485.
- [76] Afferrante, L., Carbone, G., Demelio, G., Pugno, N., 2013. Adhesion of elastic thin films: double peeling of tapes versus axisymmetric peeling of membranes. *Tribology Letters*, 52(3), 439-447.
- [77] Xia, S. M., Ponson, L., Ravichandran, G., Bhattacharya, K., 2013. Adhesion of heterogeneous thin films—I: elastic heterogeneity. *Journal of the Mechanics and Physics of Solids*, 61(3), 838-851.
- [78] Cohen N, Waite JH, McMeeking RM, Valentine MT, 2019. Force distribution and multiscale mechanics in the mussel byssus. *Philos Trans Roy Soc B*; 374(1784):20190202.
- [79] Persson, B. N. J., 2021. A simple model for viscoelastic crack propagation. *The European Physical Journal E*, 44, 1-10.